MODELING OF OVERTURNING WAVES OVER ARBITRARY BOTTOM IN A 3D NUMERICAL WAVE TANK

Stéphan T. Grilli,
Department of Ocean Engineering, University of Rhode Island, Narragansett, RI 02882, USA
Philippe Guyenne and Frédéric Dias,
Ecole Normale Supérieure (CMLA, UMR8536 CNRS), Cachan CEDEX, F-94235

Abstract

An accurate three-dimensional (3D) Numerical Wave Tank solving fully nonlinear potential flow theory is developed and validated for modeling wave propagation up to overturning over arbitrary bottom topography. The model combines a higher-order 3D-BEM and a Mixed-Eulerian-Lagrangian time updating of the free surface, based on explicit second-order Taylor series expansions, with adaptive time steps. The spatial discretization is third-order and imposes continuity of the inter-element slopes. Discretized boundary conditions at intersections between domain boundary sections (corner/edges) are well-posed in all cases of mixed Dirichlet-Neuman problems. Waves can be generated in the tank by wavemakers, or be directly specified on the free surface. If required, absorbing layers can be specified on lateral boundaries. Node regridding to a finer resolution can be specified at any time step over selected areas of the free surface. Results are presented for both validation tests with a permanent wave propagation over constant depth, and for the computation of a 3D overturning wave over a ridge.

Keywords : Numerical wave tank, shallow water wave transformations, wave breaking, coastal engineering.

INTRODUCTION

Wave propagation, up to overturning, over slopes and complex bottom features, has been successfully modeled in two-dimensional (2D) Numerical Wave Tanks (NWT), usually based on fully nonlinear potential flow equations (FNPF) expressed in a mixed Eulerian-Lagrangian formulation (MEL) (e.g., Grilli *et al.*, 1996,1997; Grilli and Horrillo, 1999). Such calculations are in good agreement with laboratory experiments for intermediate water (e.g., Dommermuth *et al.*, 1988), and for shallow slopes (e.g., Grilli *et al.*, 1997). In the more recent 2D-NWTs, incident waves can be generated at one extremity, and reflected, absorbed, or radiated at the other extremity (e.g., Grilli and Horrillo, 1997). In most cases, Laplace's equation is solved with a higher-order Boundary Element Method (BEM), either based on Green's identity or on Cauchy integral theorem. Time integration of free surface boundary conditions is performed using either a time marching predictor-corrector scheme, such as Runge-Kutta (RK) or Adams-Bashforth-Moulton (ABM) (e.g., Dommermuth *et al.*, 1988), or a Taylor series expansion method (e.g., Grilli *et al.*, 1989).

Although several 3D-NWTs have been developed for non-overturning waves over constant depth (e.g., Romate, 1989; Boo *et al.*, 1994; Ferrant, 1998; Celebi *et al.*, 1998), only a few attempts have been reported, which solved 3D-FNPF problems for overturning waves. Xü and Yue (1992) calculated 3D overturning waves, in a doubly-periodic computational domain with infinite depth (i.e., only the free surface was discretized). Two-dimensional periodic waves were made to break by specifying an asymmetric surface pressure. A higher-order BEM was implemented, based on Green's identity, with a doubly periodic Green's function in horizontal directions x and y, quadratic isoparametric boundary elements, and a RK-ABM time stepping. Sawtooth-instabilities eventually developed near wave crests; these were eliminated by smoothing, typically applied every few time steps. Broeze (1993) developed a numerical model similar to Xü and Yue's, but for non-periodic domains and finite depth, and was able to produce the initial stages of wave overturning over a bottom shoal; numerical instabilities were also experienced, which limited computations.

Based on the limited discussion above (more details can be found in the recent review of 2D and 3D NWTs by Kim *et al.*, 1999), it appears that FNPF theory is accurate for modeling overturning waves over arbitrary bottom. Many 2D and a few 3D models (i.e., NWTs) of that problem have been proposed. Among these, the most stable and accurate models were clearly those in which higher-order spatial and temporal discretizations schemes were used, and important problems such as corner/edge boundary conditions and numerical integrations were carefully addressed. Importantly, in the few existing higher-order 2D models, strongly nonlinear waves were accurately propagated over long distances and/or time, up to overturning, without need for smoothing or filtering of the solution (e.g., Grilli *et al.*, 1996,1997). The nonlinear nature of the problem and lack of dissipation in FNPF theory indeed are such that numerical errors, even very small, remain integral part of the solution and build up as a function of time, through superposition and nonlinear interactions. Therefore, such errors must be minimized by seeking optimum accuracy in all numerical aspects of the model.

In the present study, the experience gained by the authors in developing accurate and stable numerical methods for 2D-FNPF-NWTs is applied to the development of a new, similarly accurate, 3D-FNPF-NWT for overturning waves. The NWT is developed using a higher-order 3D-BEM and a MEL time updating, based on second-order Taylor series expansions, with adaptive time steps, similar to that used in Grilli *et al.*'s 2D model. The NWT is applicable to nonlinear wave transformations, up to overturning and breaking, from deep to shallow water over arbitrary bottom topography. Arbitrary waves can be generated in the NWT (by wavemakers or directly on the free surface). Reflective or absorbing boundary conditions are implemented on lateral boundaries of the NWT; for the latter, on a way similar to Grilli and Horrillo (1997). Geometry and field variables are represented on the NWT boundary by 16-node cubic "sliding" two-dimensional elements similar, in principle, to the one-dimensional 4-node "Middle-Interval-Interpolation (MII)" elements introduced by Grilli and Subramanya (1996) in their 2D model; such elements provide local inter-element

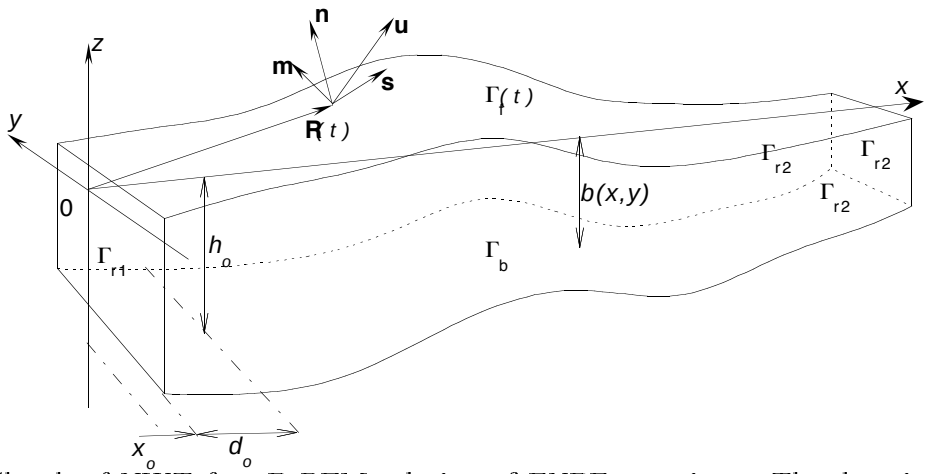

Fig. 1 : Sketch of NWT for 3D-BEM solution of FNPF equations. The domain is defined for $x \geq x_o$. Note a region of constant depth $h = h_o$ is specified for $x \leq x_o + d_o$, beyond which depth is set to $h = b(x, y)$. Tangential vectors at point $\mathbf{R}(t)$ of the free surface $\Gamma_f(t)$ are defined as $(\mathbf{s}, \mathbf{m})$ and outward normal vector as $\mathbf{n}$.

continuity of the first and second derivatives. Accurate and efficient numerical integrations are developed for these elements. Discretized boundary conditions at intersections (corner/edges) between the free surface or the bottom, and lateral boundaries, are well-posed in all cases of mixed boundary conditions, following the methods introduced by Grilli and Svendsen (1990) and Grilli and Subramanya (1996). Higher-order tangential derivatives required for the time updating are calculated in a local curvilinear coordinate system using two-dimensional 25-node sliding 4th-order elements similar, in principle, to the 5-node one-dimensional elements introduced by Grilli and Svendsen (1990) for calculating s-derivatives in their 2D model. Node regridding to a higher resolution can be specified over selected areas of the free surface. Details of the model development and applications are given in the following.

THE MODEL

Governing equations and boundary conditions

Equations for fully nonlinear potential flows with a free surface are summarized below. The velocity potential $\phi(\mathbf{x}, t)$ is used to represent inviscid irrotational 3D flows in Cartesian coordinates $\mathbf{x} = (x, y, z)$, with z the vertical upward direction (and $z = 0$ at the undisturbed

free surface; Fig. 1), and the velocity is defined by, $\mathbf{u} = \nabla\phi = (u, v, w)$.

Continuity equation in the fluid domain $\Omega(t)$, with boundary $\Gamma(t)$, is a Laplace's equation for the potential,

$$\nabla^2\phi = 0 \qquad \text{in } \Omega(t) \tag{1}$$

The 3D free space Green's function for Eq. (1) is defined as,

$$G(\mathbf{x}, \mathbf{x}_l) = \frac{1}{4\pi r} \quad , \text{with} \quad \frac{\partial G}{\partial n}(\mathbf{x}, \mathbf{x}_l) = -\frac{1}{4\pi}\frac{\mathbf{r}\cdot\mathbf{n}}{r^3} \quad , \tag{2}$$

$\mathbf{r} = \mathbf{x} - \mathbf{x}_l$, and $r = \mid \mathbf{r} \mid$ the distance from point $\mathbf{x}$ to the reference point $\mathbf{x}_l = (x_l, y_l, z_l)$, both on boundary Γ, and $\mathbf{n}$ the outward normal unit vector to the boundary at point $\mathbf{x}$.

Green's second identity transforms Eq. (1) into the Boundary Integral Equation (BIE),

$$\alpha(\mathbf{x}_l)\,\phi(\mathbf{x}_l) = \int_{\Gamma(\mathbf{x})} \left\{ \frac{\partial\phi}{\partial n}(\mathbf{x})\, G(\mathbf{x}, \mathbf{x}_l) - \phi(\mathbf{x})\, \frac{\partial G}{\partial n}(\mathbf{x}, \mathbf{x}_l) \right\} \mathrm{d}\Gamma \tag{3}$$

in which $\alpha(\mathbf{x}_l) = \theta_l/(4\pi)$, with θ_l the exterior solid angle made by the boundary at point $\mathbf{x}_l$ (i.e., 2π for a smooth boundary).

The boundary is divided into various sections, with different boundary conditions (Fig. 1). On the free surface $\Gamma_f(t)$, ϕ satisfies the nonlinear kinematic and dynamic boundary conditions,

$$\frac{D\,\mathbf{R}}{D\,t} = \mathbf{u} = \nabla\phi \qquad \text{on } \Gamma_f(t) \tag{4}$$

$$\frac{D\,\phi}{D\,t} = -gz + \frac{1}{2}\,\nabla\phi\cdot\nabla\phi - \frac{p_a}{\rho} \qquad \text{on } \Gamma_f(t) \tag{5}$$

respectively, with $\mathbf{R}$ the position vector of a free surface fluid particle, g the acceleration due to gravity, p_a the atmospheric pressure, ρ the fluid density, and D/Dt the material derivative.

Various methods can be used in the model for wave generation. When waves are generated by simulating a wavemaker motion on the "open sea" boundary of the computational domain, $\Gamma_{r1}(t)$, motion and velocity $[\mathbf{x}_p, \mathbf{u}_p]$ are specified over the wavemaker as,

$$\overline{\mathbf{x}} = \mathbf{x}_p \qquad \text{and} \qquad \overline{\frac{\partial\phi}{\partial n}} = \mathbf{u}_p\cdot\mathbf{n} \qquad \text{on } \Gamma_{r1}(t) \tag{6}$$

where overlines denote specified values.

Along the bottom Γ_b and other stationary parts of the boundary, referred to as Γ_{r2}, a no-flow condition is prescribed as,

$$\overline{\frac{\partial \phi}{\partial n}} = 0 \qquad \text{on } \Gamma_b \text{ and } \Gamma_{r2} \tag{7}$$

For well-posed problems, we have, $\Gamma \equiv \Gamma_f \cup \Gamma_{r1} \cup \Gamma_{r2} \cup \Gamma_b$.

Time integration

Free surface boundary conditions (4) and (5) are integrated at time t to establish both the new position and the boundary conditions on the free surface $\Gamma_f(t)$ at a subsequent time $(t + \Delta t)$ (with Δt a varying time step).

Following the method implemented in Grilli *et al.*'s (1989,1996) 2D model, second-order explicit Taylor series expansions are used to express both the new position $\mathbf{R}(t + \Delta t)$ and the potential $\phi(\mathbf{R}(t + \Delta t))$ on the free surface, in a MEL formulation,

$$\overline{\mathbf{R}}(t + \Delta t) = \mathbf{R}(t) + \Delta t \frac{D\,\mathbf{R}}{D\,t}(t) + \frac{(\Delta t)^2}{2}\frac{D^2\mathbf{R}}{Dt^2}(t) + \mathcal{O}[(\Delta t)^3] \tag{8}$$

$$\overline{\phi}(\mathbf{R}(t + \Delta t)) = \phi(t) + \Delta t \frac{D\,\phi}{D\,t}(t) + \frac{(\Delta t)^2}{2}\frac{D^2\phi}{Dt^2}(t) + \mathcal{O}[(\Delta t)^3] \tag{9}$$

Coefficients in these Taylor series are expressed as functions of the potential, its partial time derivative, and the normal and tangential derivatives of both of these along the free surface. As in the 2D-NWT by Grilli *et al.*, time step Δt is adapted at each time as a function of the minimum distance between 2 nodes on the free surface and a constant mesh Courant number $\mathcal{C}_o \simeq 0.5$. [Tests performed with this model, for solitary waves, showed that a value $\mathcal{C}_o = 0.4 - 0.5$ leads to minimum errors in mass and energy conservation, for a given spatial discretization.]

First-order coefficients are given by Eqs. (4) and (5), which requires calculating $(\phi, \frac{\partial \phi}{\partial n})$ on the free surface; this is done by solving Eq. (3) at time t, with boundary conditions (6), (7) and (9). Second-order coefficients are obtained from the material derivative of Eqs. (4) and (5), which requires also calculating $(\frac{\partial \phi}{\partial t}, \frac{\partial^2 \phi}{\partial t \partial n})$ at time t; this is done by solving a BIE

similar to Eq. (3) for these fields. The free surface boundary condition for this second BIE is obtained from Bernoulli Eq. (4), after solution of the first BIE for ϕ as,

$$\overline{\frac{\partial \phi}{\partial t}} = -gz - \frac{1}{2}\nabla\phi \cdot \nabla\phi - \frac{p_a}{\rho} \qquad \text{on } \Gamma_f(t) \tag{10}$$

For a wave generation by a wavemaker, Eq. (6) gives,

$$\overline{\frac{\partial^2 \phi}{\partial t \partial n}} = \frac{\partial(\mathbf{u}_p \cdot \mathbf{n})}{\partial t} \qquad \text{on } \Gamma_{r1}(t) \tag{11}$$

and for the bottom and other stationary boundaries,

$$\overline{\frac{\partial^2 \phi}{\partial t \partial n}} = 0 \qquad \text{on } \Gamma_b \text{ and } \Gamma_{r2} \tag{12}$$

Advantages of this time stepping scheme are of being explicit and using spatial derivatives of the field variables along the free surface in the calculation of values at $(t + \Delta t)$. This provides a better stability of the computed solution and makes it possible to use larger time steps, for a similar accuracy, than in RK or predictor-corrector methods, which only use point to point updating based on time derivatives, and are thus more subject to sawtooth instabilities. Hence, this also makes the overall solution more efficient.

Tangential derivatives

For calculating tangential derivatives, e.g., needed to calculate coefficients in Eqs. (8) and (9), a local curvilinear coordinate system $(\mathbf{s}, \mathbf{m}, \mathbf{n})$ is defined at each boundary node (Fig. 1), with $\mathbf{s} = \mathbf{x}_s$, $\mathbf{m} = \mathbf{x}_m$, and $\mathbf{n} = \mathbf{s} \times \mathbf{m}$ (subscripts indicate partial derivatives). Derivatives of the geometry and field variables in tangential directions $\mathbf{s}$ and $\mathbf{m}$ are computed, by defining, around each node a local 5 by 5 node, 4th-order, sliding element $\mathbf{x}(\xi, \eta)$, and differentiating within it. Hence, we find,

$$\mathbf{u} = \nabla\phi = \phi_s\,\mathbf{s} + \phi_m\,\mathbf{m} + \phi_n\,\mathbf{n} \tag{13}$$

where ϕ_s and ϕ_m denote tangential velocities. Using Eq. (13), Laplace's Eq. (1) can be expressed as,

$$\begin{aligned} \phi_{nn} \;=\; & -\phi_{ss} - \phi_{mm} + \phi_s\{\mathbf{x}_{ss}\cdot\mathbf{s} - \mathbf{x}_{sm}\cdot\mathbf{m}\} + \phi_m\{\mathbf{x}_{mm}\cdot\mathbf{m} - \mathbf{x}_{sm}\cdot\mathbf{s}\} \\ & + \phi_n\{\mathbf{x}_{ss}\cdot\mathbf{n} + \mathbf{x}_{mm}\cdot\mathbf{n}\} \end{aligned} \tag{14}$$

and the particle acceleration, i.e. the second-order term in Eq. (8), as,

$$\frac{D\,\mathbf{u}}{D\,t} =$$

$$\mathbf{s}\left\{\phi_{ts}+\phi_s\phi_{ss}+\phi_m\phi_{sm}+\phi_n\phi_{ns}-\phi_s^2\{\mathbf{x}_{ss}\cdot\mathbf{s}\}+\phi_m^2\{\mathbf{x}_{mm}\cdot\mathbf{s}\}-\phi_n\phi_m\{\mathbf{x}_{sm}\cdot\mathbf{n}\}\right\}$$

$$+\mathbf{m}\left\{\phi_{tm}+\phi_s\phi_{sm}+\phi_m\phi_{mm}+\phi_n\phi_{nm}+\phi_s^2\{\mathbf{x}_{ss}\cdot\mathbf{m}\}-\phi_m^2\{\mathbf{x}_{mm}\cdot\mathbf{m}\}-\phi_n\phi_s\{\mathbf{x}_{sm}\cdot\mathbf{n}\}\right\}$$

$$+\mathbf{n}\left\{\phi_{tn}+\phi_s\phi_{ns}+\phi_m\phi_{nm}-\phi_n\{\phi_{ss}+\phi_{mm}\}+\phi_s^2\{\mathbf{x}_{ss}\cdot\mathbf{n}\}+\phi_m^2\{\mathbf{x}_{mm}\cdot\mathbf{n}\}+2\phi_s\phi_m\{\mathbf{x}_{sm}\cdot\mathbf{n}\}\right.$$

$$\left.+\phi_n^2\{\mathbf{x}_{ss}\cdot\mathbf{n}+\mathbf{x}_{mm}\cdot\mathbf{n}\}+\phi_n\phi_s\{\mathbf{x}_{ss}\cdot\mathbf{s}-\mathbf{x}_{sm}\cdot\mathbf{m}\}+\phi_n\phi_m\{\mathbf{x}_{mm}\cdot\mathbf{m}-\mathbf{x}_{sm}\cdot\mathbf{s}\}\right\} \quad (15)$$

Finally, the second-order term in Eq. (9) is given by,

$$\frac{D^2\phi}{Dt^2} = -g\,w + \mathbf{u}\cdot\frac{D\,\mathbf{u}}{D\,t} - \frac{1}{\rho}\frac{D\,p_a}{D\,t} \quad (16)$$

where Eqs. (13) and (15) are used to calculate the second term in the right hand side, and w denotes the vertical particle velocity.

Finally for a plane wavemaker boundary on $\Gamma_{r1}(t)$, using Eqs. (13) and (14), Eq. (11) becomes,

$$\overline{\frac{\partial^2\phi}{\partial t\partial n}} = (\dot{\mathbf{u}}_p\cdot\mathbf{n}) + (\mathbf{u}_p\cdot\frac{D\,\mathbf{n}}{D\,t}) + (\mathbf{u}_p\cdot\mathbf{n})\{\phi_{ss}+\phi_{mm}\} - \phi_s\phi_{ns}-\phi_m\phi_{nm} \quad (17)$$

where, $\dot{\mathbf{u}}_p$ denotes the absolute wavemaker acceleration, and $D\mathbf{n}/Dt = \omega\times\mathbf{n}$, for a wavemaker rotating with angular velocity ω.

Discretization, numerical integrations, regridding

The BIEs for ϕ and $\frac{\partial\phi}{\partial t}$ are solved by a Boundary Element Method (BEM). The boundary is discretized into collocation nodes and higher-order elements are used to interpolate in between m of these nodes. Within each element, the boundary geometry and the field variables (denoted by $u=\phi$ and $q=\frac{\partial\phi}{\partial n}$ for simplicity) are discretized using polynomial shape functions. These are analitically defined over a single reference element of intrinsic coordinates $(\xi,\eta)\in[-1,1]$. Variations of the geometry and field variables over each element

k are described by their nodal values, $\mathbf{x}_j^k$, u_j^k and q_j^k, and by the local shape functions $N_j(\xi,\eta)$ as,

$$\mathbf{x}(\xi,\eta) = N_j(\xi,\eta)\,\mathbf{x}_j^k \tag{18}$$

$$u(\xi,\eta) = N_j(\xi,\eta)\,u_j^k \qquad \text{and} \qquad q(\xi,\eta) = N_j(\xi,\eta)\,q_j^k \tag{19}$$

where $j = 1,\ldots,m$, numbers the nodes within each element $k = 1,\ldots,M_\Gamma$, and the summation convention is applied to repeated subscripts.

Isoparametric elements can provide a high-order approximation within their area of definition but only offer C_0 continuity of the geometry and field variables at nodes in between elements. Based on the experience acquired in modeling overturning waves with 2D-NWTs, for producing stable accurate results, one needs to define elements which are both higher-order within their area of definition, and at least locally C_2 continuous in between elements. To do so, various methods were implemented and tested in 2D-NWTs. Here, elements are defined using an extension of the so-called Middle-Interval-Interpolation (MII) method introduced by Grilli and Subramanya (1996). Boundary elements are 4-nodes quadrilaterals, with cubic shape functions defined using both these and additional neighboring nodes in each direction, for a total of $m = 16$ nodes. Hence, only part of the interval of variation (usually the middle part, unless nodes are close to a boundary intersection) of the cubic shape functions is used for calculating the boundary integrals in Eq. (3).

Details of curvilinear changes of variables needed for expressing boundary integrals over MII reference elements, treatments of corners and boundary intersections, and final dicretized equations, are left out due to lack of space.

Discretized boundary integrals are calculated for each collocation node by numerical integration. When collocation node l does not belong to the integrated quadrilateral element (i.e., $l \neq j(k) = 1,\ldots,4$), a standard Gauss-Legendre quadrature method is used. When node l does belong to the element, distance r in the Green's function, and its normal gradient, becomes zero at one of the nodes of the element (Eq. (2)). It can be shown, in this case, that

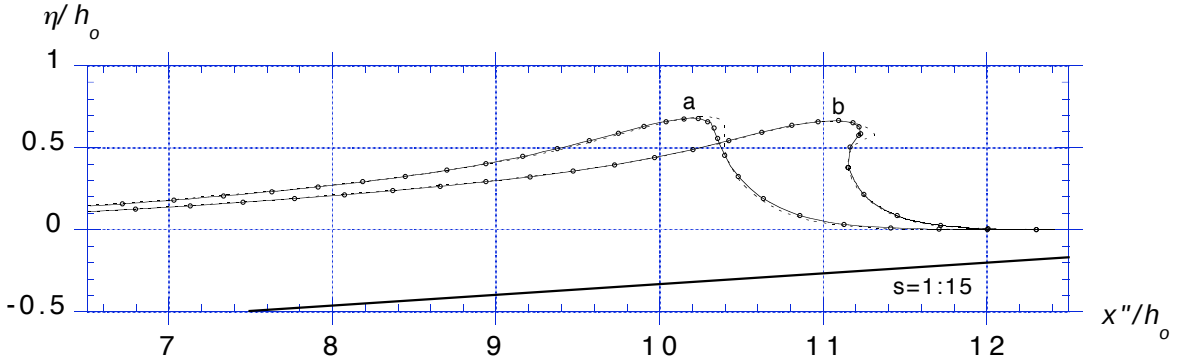

Fig. 2 : Comparison of 3D (—○—) and 2D (- - - -) results (Grilli *et al.*, 1997) for the shoaling of a solitary wave of height $H_o/h_o = 0.6$ over a slope s =1:15, at times $t' =$ a : 7.551; and b: 8.163.

integrals including G are weakly singular (and thus integrable), whereas integrals including G_n are non-singular. For the former integrals, new methods of "singularity extraction", well-suited to MII elments, were developed based on polar coordinate and other transformations; again, details are left out due to lack of space.

Finally, a two-dimensional regridding method is implemented for the free surface, based on a reinterpolation of nodes for equally spaced MII elements in the x and y directions. Thus, this method assumes a single-valued free surface $\eta(x, y)$ at the time of regridding.

APPLICATIONS

Solitary wave shoaling over a plane slope

Grilli *et al.* (1997) calculated the shoaling and breaking of solitary waves over plane slopes in their 2D-FNPF-NWT and compared results to detailed laboratory experiments. They showed that computations of surface elevations matched experimental results within two percent, up to the breaking point.

To validate the 3D model, similar computations are made in a quasi-2D narrow domain of width $2h_o$, having a plane slope s =1:15, starting at $d'_o = 5.4$ in depth $h'_o = 1$ and truncated at $x' = 18$ in depth $h' = 0.16$ (Fig. 1; dashes indicate non-dimensional variables based on long wave theory). The initial wave is an exact FNPF solitary wave of height $H'_o = 0.6$, with its crest located at $x' = 5.5$ for $t' = 0$. The initial BEM discretization has 60 by 4

quadrilateral elements in the x and y directions, respectively (node spacing, $\Delta x'_o = 0.30$ and $\Delta y'_o = 0.50$), on the bottom and free surface boundaries. The lateral boundaries Γ_{r2} have grid lines connecting the free surface and bottom edge nodes, with 4 elements specified in the vertical direction along each pair of connecting lines. The total number of nodes in the NWT is 1270 and the number of quadrilateral MII elements is 992 (630" CPU time per time step on a Mac G3-266). The initial time step is set to $\Delta t'_o = 0.14$ and, hence, $\mathcal{C}_o = 0.47$.

Fig. 2 shows a comparison between a cross-section in the 3D results, at $y' = 0$ (horizontally shifted to $x'' = x' - d'_o$), with the 2D results calculated by Grilli *et al.* (1997). Curve a corresponds to the break point in the 2D model, i.e., when a vertical tangent occurs on the front face; the agreement between 3D and 2D results is quite good, except at the tip of the crest, likely due to the coarser discretization in the 3D-NWT (about 2 times coarser in the x direction than for the 2D case). At the time of curve a, numerical errors on wave mass and energy conservation are quite small (0.056 % and 0.117 %, respectively). Due to node convergence at the wave crest, the time step has reduced to $\Delta t' = 0.0259$. In curve b, the wave crest starts overturning, but the agreement of 3D and 2D results is still good. Errors on wave mass and energy conservation are still small (0.106 % and 0.351 %, respectively) but the time step has considerably reduced to $\Delta t' = 0.0085$. Beyond this stage, however, 3D computations quickly fail, as elements start overlapping on the lateral vertical boundaries of the NWT, at $y' = \pm 1$. This limitation could be eliminated by implementing appropriate regridding techniques for the elements on the sidewalls of the NWT.

Solitary wave shoaling and breaking over a sloping ridge

A truly three-dimensional overturning wave is now produced in a wider NWT, of width $4h_o$ in the y direction, with a sloping ridge at its extremity. The ridge starts at $x' = 5.225$ and has a 1:15 slope in the middle ($y = 0$), tapered in the y direction by specifying a depth variation in the form of a sech^2 modulation. The ridge is truncated at $x' = 19$, where the minimum depth is $h' = 0.067$ in the middle part ($y' = 0$), and the maximum depth $h' = 0.617$

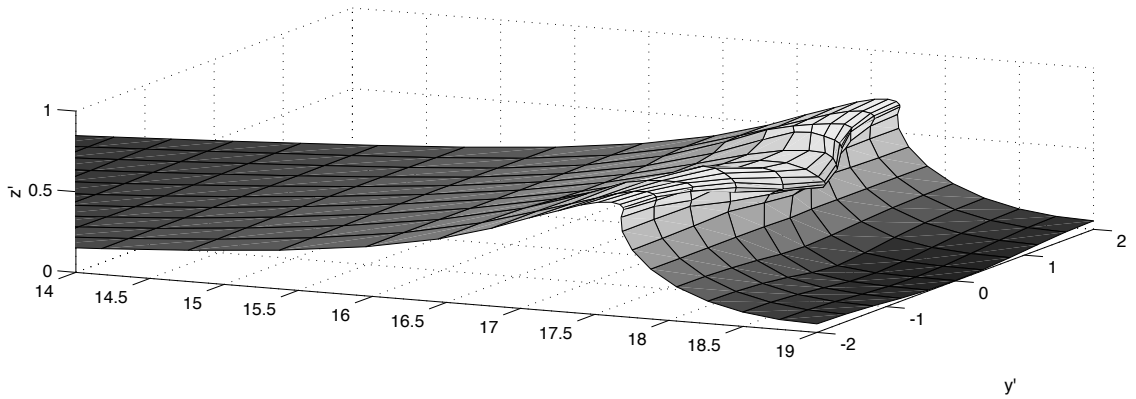

Fig. 3 : Same case as Fig.2 but over a ridge modeled as a sloping bottom s =1:15, with a sech^2 modulation in y. The region for $x/h_o > 7.2$ was regridded to equal intervals. Results are for time $t' = 9.196$.

on the sides ($y' = \pm 2$). The same solitary wave as before is used, with $H'_o = 0.6$ and the crest being located at $x' = 5.7$ for $t' = 0$.

The initial BEM discretizations on the bottom and free surface have 40 by 8 quadrilateral elements in the x and y directions, respectively (node spacing, $\Delta x'_o = 0.475$ and $\Delta y'_o = 0.50$). Lateral boundaries again have 4 elements in the vertical direction. The total number of nodes is 1238 and the number of quadrilateral MII elements is 1024 (600" CPU time per time step on a Mac G3-266). The initial time step is set to $\Delta t'_o = 0.214$ and, hence, $\mathcal{C}_o = 0.45$. Maximum numerical errors of 1 % on wave mass and energy conservation were deemed acceptable in this application. Computations were first performed in the initial discretization, up to reaching these maximum errors ($t' = 8.788$). Regridding of part of the NWT to a finer discretization was then specified at an earlier time ($t' = 6.000$) for which errors were very small (0.065 % and 0.045 %, respectively). At this stage, the wave crest was located at $x' = 14.203$, with $H' = 0.644$. The regridded discretization was increased to 40 by 10 quadrilateral elements on the free surface and bottom boundaries, for $x' = 8.075$ to 19 (with $\Delta x'_o = 0.273$ and $\Delta y'_o = 0.40$; total number of nodes 1422, and elements 1200, with 735 sec CPU per time step), and computations were restarted up to reaching the maximum errors ($t' = 9.196$, and the time step has reduced to $\Delta t' = 0.0051$).

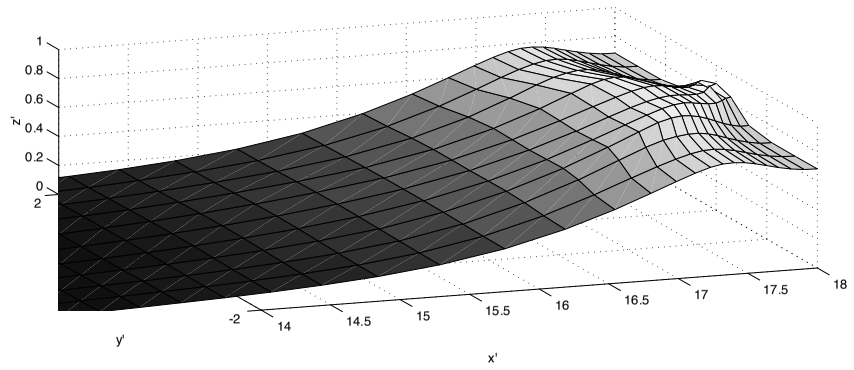

Fig. 4 : Same case as Fig. 3, at time $t' = 9.079$, but with a vertical wall located at $x' = 18$.

Fig. 3 shows the wave computed at that stage. The error on wave energy conservation reaches the maximum (1 %), and the mass conservation error is 0.164 %. Wave overturning is well developed in the middle of the NWT but, in fact, we see that it has already reached the sidewalls, at $y = \pm 2$, where elements start wrapping up. Hence, computations cannot be pursued much beyond this stage. This limitation, again, could be eliminated by either using proper regridding on the sidewall boundaries, or by using a even wider NWT, in which wave overturning would occur for a longer time in the middle part of the tank, before reaching the sidewalls. Such results, which require much larger discretizations and the use of a supercompiuter, will be presented during he conference.

Solitary wave shoaling and impact on a vertical wall

To illustrate the ability of the model to calculate violent 3D wave impact on structures, the end vertical boundary of the NWT was moved back to $x' = 18$ and the same case as in the previous section was recalculated. Fig. 4 shows results for $t' = 9.079$ in the regridded discretization. For smaller times, the wave almost reaches overturning but, instead, experiences a so-called "flip-through" motion in the middle part of the tank, in which the water line on the wall rapidly shuts upwards.

Unlike with 2D calculations (Cooker and Peregrine, 1992), however, due to 3D effects,

runup on the wall is initially faster close to the sidewalls ($y = \pm 2$) than in the middle of the tank. Hence, this creates lateral flows moving from the deeper parts toward the middle of the NWT, thus focusing the wave impact around ($y = 0$), in the shallower water region over the ridge. The strong flow convergence from three major directions creates a local jet moving along the wall with large upward vertical acceleration. No attempt to better resolve this jet, in space and time, by regridding to an even finer discretization, was made and the figure shows results at the instant maximum error on wave energy conservation was reached for the specified discretization (0.95 %). At this time, the error on wave mass conservation was 0.26 %.

CONCLUSIONS

A new 3D-NWT solving FNFP equations based on a higher-order BEM was implemented and validated. The NWT is applied to modeling wave shoaling and overturning over a sloping bottom. Overall, results show a better stability and numerical accuracy than in previous attempts reported in the literature for calculating such strongly nonlinear 3D surface waves. Cases of wave overturning over arbitrary bottom topography are presented which, to our knowledge, was never attempted in a general 3D-NWT.

ACKNOWLEDGMENTS

The first author acknowledges support from the US Office of Naval Research, under grant N-00014-99-10439 of the Coastal Dynamics Division (code 321 CD). The second and third authors acknowledge support from the Direction Générale de l'Armement (France). Computations presented in this work were performed in part on the IDRIS CRAY C90 supercomputer, under CNRS funding.

REFERENCES

Broeze, J. (1993). *Numerical Modelling of Nonlinear Free Surface Waves With a 3D Panel Method.* Ph.D. Dissertation, Enschede, The Netherland.

Boo, S.Y., Kim, C.H. and Kim, M.H. (1994). "A Numerical Wave Tank for Nonlinear Irregular Waves by 3D Higher-order Boundary Element Method." *Intl. J. Offshore and Polar Engng.*, Vol 4(4), pp 265-272.

Celebi, M.S., Kim, M.H. and Beck, R.F. (1998). "Fully Nonlinear 3D Numerical Wave Tank Simulations." *J. Ship Res.,* Vol 42(1), pp 33-45.

Cooker, M.J. and D.H., Peregrine (1992). "Wave Impact Pressure and its Effect Upon Bodies Lying on the Sea Bed." *Coastal Engng.,* Vol 18, pp 205-229.

Dommermuth, D.G., Yue, D.K.P., Lin, W.M., Rapp, R.J., Chan, E.S. and W.K., Melville (1988). "Deep-water Plunging Breakers : a Comparison Between Potential Theory and Experiments." *J. Fluid Mech.,* Vol 189, pp 423-442.

Ferrant, P. (1998). "Runup on a Cylinder due to Waves and Currents : Potential Flow Solution with Fully Nonlinear Boundary Conditions." In *Proc. 8th Intl. Offsh. Polar Engng. Conf.,* Vol 3, pp 332-339.

Grilli, S.T. and Horrillo, J. (1997). "Numerical generation and absorption of fully nonlinear periodic waves," *J. Engng. Mech.*, Vol 123(10), pp 1060-1069.

Grilli, S.T. and Horrillo, J. (1999) "Shoaling of periodic waves over barred-beaches in a fully nonlinear numerical wave tank." Intl. J. Offshore and Polar Engng., Vol 9(4), pp 257-263.

Grilli, S.T., Skourup, J., and Svendsen, I.A. (1989). "An efficient boundary element method for nonlinear water waves," *Engng. Analysis with Boundary Elements*, Vol 6(2), pp 97-107.

Grilli, S.T. and I.A., Svendsen (1990). Corner Problems and Global Accuracy in the Boundary Element Solution of Nonlinear Wave Flows. *Engng. Analysis with Boundary Elements.*, Vol 7(4), pp 178-195.

Grilli, S.T. and Subramanya, R. (1996). "Numerical modeling of wave breaking induced by fixed or moving boundaries." *Computational Mech.*, Vol 17, pp 374-391.

Grilli, S., Svendsen, I.A. and Subramanya, R. (1997). "Breaking Criterion and Characteristics for Solitary Waves on Slopes." *J. Waterway Port Coastal and Ocean Engng.,* Vol 123(3), pp 102-112.

Kim, C.H., Clément, A.H. and Tanizawa, K. (1999). "Recent Research and Development of Numerical Wave Tank—A review." *Intl. J. Offshore and Polar Engng.*, Vol 9(4), pp 241-256.

Romate, J.E., (1989). *The Numerical Simulation of Nonlinear Gravity Waves in Three Dimensions using a Higher Order Panel Method.* Ph.D. Dissertation. Department of Applied Mathematics, University of Twente, The Netherland.

Xü, H. and D.K.P., Yue (1992). "Numerical Study of Three dimensional overturning waves." In *Proc. 7th Intl. Workshop on Water Waves and Floating Bodies* (Val de Reuil, France, May 1992), R. Cointe (ed.), pp 303-307.